Ahmed E. Abouelregal · Hamid M. Sedighi
Victor A. Eremeyev

Thermomagnetic behavior of a semiconductor material heated by pulsed excitation based on the fourth-order MGT photothermal model

Abstract This article proposes a photothermal model to reveal the thermo-magneto-mechanical properties of semiconductor materials, including coupled diffusion equations for thermal conductivity, elasticity, and excess carrier density. The proposed model is developed to account for the optical heating that occurs through the semiconductor medium. The Moore–Gibson–Thompson (MGT) equation of the fourth-order serves as the theoretical framework to establish the photothermal model. It is well-known that the optical and heat transfer properties of such materials behave as random functions of photoexcited-carrier density; therefore, the current model is remarkably more reliable compared to the earlier closed-form theories which are limited to a single form. The constructed theoretical framework is able to investigate the magneto-photo-thermoelastic problems in a semiconductor medium due to laser pulse excitation as a case study. Some parametric studies are used to exhibit the impact of thermal parameters, electromagnetic fields, laser pulses and thermoelectric coupling factors on the thermomagnetic behavior of physical variables. Finally, several numerical examples have been presented to draw the distributions of the examined field variables.

Keywords MGT thermoelasticity · Photoexcited · Semiconductor · Laser pulse

1 Introduction

A semiconductor material is a substance that possesses the electrical conductivity properties somewhere between a conductor and non-conductor or insulator materials. This indicates that semiconductors can switch

between conducting and insulating behavior depending on the environmental circumstances. Silicon is the most well-known pure semiconductor whereas the gallium arsenide is an example of a compound semiconductor element. Semiconductor gain mechanisms with ultrafast time scales have emerged as a hot topic in the scientific community during the past few decades. To this end, several experimental procedures have been conducted to examine the behavior of semiconductor laser amplifiers in response to ultrashort (picosecond or shorter time scales) light pulses in this area. Complexity in gain, measured as a timescale in the order of a picosecond, has been revealed in the empirical tests. Mathematical computations support the assumption that the peculiar behavior of carrier ensemble on short time scales, particularly the conduction of dynamic carrier heating, is responsible for this form of gain responses [1].

Research into the characteristics of semiconductors began around the end of the nineteenth century. Semiconductors had extraordinary use across many sectors in the 20th century as a result of technological and industrial advancements including incorporating anything from medical equipment to electrical circuits and even solar cells that generate renewable energy. Researchers who worked on semiconductor implants realized that the internal systems of these substances may change with temperature, particularly when subjected to light or a laser beam [2]. Heat generation is a common side effect of irradiating a semiconductor with a powerful laser beam. Since the most of the light energy that a semiconductor receives first goes to free electrons and hole systems, the way that free carriers move back and forth together is also essential to understand how well the material absorbs the laser energy [3]. As they relate to device quality and performance, heat transfer characteristics are very important features in semiconductor laser interactions. Semiconductor is widely used in optical communication systems and energy pumping, where the laser must operate with pulsed excitations. In the case of lasers excited by periodic pulses, heat buildup in the active area can develop if the temperature of the active region does not drop to the temperature of the heat sink before when another cycle begins. To make the optimum use of laser diode's power output, the characteristics of thermodynamic responses especially the thermal time constant are necessary [4].

The primary application of semiconductors is to fabricate semiconductor devices, which are fundamental to a wide range of electronic products. Electrons used to be able to move around freely in a vacuum and semiconductor devices are currently used almost everywhere. The diode is a semiconductor component that works as a one-way valve in a circuit, permitting only the flow of electricity in one direction. Instead, conductors are conductive in both ways. Transistors are built with semiconductors and are utilized for quick switching and current amplification. Most semiconductors are MOSFETs, which stands for metal-oxide-semiconductor field-effect transistor [5]. The applications of semiconductors in electronics is ubiquitous. Semiconductor components like integrated circuits, diodes and transistors are essential for the operation of many common household appliances, including mobile phones, computers, gaming consoles, microwaves and refrigerators. Embedded systems are little computers designed to function within a larger system. They have the power to operate the gadget and make it possible for the user to have input. The majority of technology we are daily relying on are embedded devices, from our thermostats and central heating to our digital watches and navigation systems to our fitness trackers and even televisions and automobile engine control units. Depending on the corresponding application, semiconductors with high thermal conductivity can be employed as a cooling agent due to their ability to dissipate heat. Some semiconductors, typically those that are accessible in liquid or amorphous form as a thin-coated film, may create light and are utilized in LEDs and OLEDs. Silicon is the most commonly utilized semiconductor in manufacturing solar panel cells. As one can see, semiconductors play a crucial part in the electrical gadgets we use or come into contact with daily, making them essential to our contemporary ways of life [6–9].

It is important to note that while researching the properties of semiconductors, it was discovered that the excited electrons are scattered toward the surface of the semiconductor and move around, causing an electron cloud known as carrier density (plasma). This electron cloud is responsible for the diffusion treats that lead to the flow of electric current, and this discovery is important in this context. In addition, when electrons flow through a material, they leave holes behind as they behave as part of the recombination process; this can also apply to the time when the electrons are moving in the form of a cloud. In recent years, thermo-optical theory has become a useful tool to describe the system of equations in such circumstances, which often occur during the hole diffusion processes. Furthermore, the concept of thermoelasticity can be implemented and introduced in this field to describe the thermoelastic deformation processes for such kind of semiconducting materials [10]. Despite the interest in examining the effect of carrier heating on gain dynamics, the dynamic behavior of carrier temperature is rarely studied. Generally, carrier temperature is only mentioned when trying to provide a makeshift justification for the gain's nonlinear nature. However, the gain determines how well an external signal may heat the carriers, and variations in the improvement also affect the carrier temperature.

Neither of the two phenomena predicted by the conventional uncoupled theory of thermoelasticity are consistent with the experimental results. To begin with, there are no elastic factors in the heat equation of the mentioned hypothesis. Second, according to the parabolic heat equation, heat waves are expected to travel at limitless speeds. For this reason, Biot [11] established the concept of coupled thermoelasticity to resolve the seeming inconsistency between the uncoupled classical theory and the experimental findings, which describes that variations in elastic properties have no discernable impact on the temperature. Contrary to the empirical evidences, limitless speeds of heat wave transmission are predicted by heat equations of diffusion type models. The generalized thermoelastic theories have been propounded by Lord and Shulman [12] and Green and Lindsay [13], who created the foundation of the dynamically coupled concepts of thermoelasticity. These models consider the propagation of heat in terms of waves rather than diffusion, making possible the prediction of heat transfer rate.

In the context of modifying the models of thermoelasticity, three developed theories with or without energy dissipation were suggested by Green and Naghdi [14–16]. The second and third types of Green and Naghdi theory are the most relevant ones in recent studies. The second type of Green and Naghdi theory is slightly different from previous models where they do not account for the thermal energy dissipation but rather incorporates the isothermal displacement gradients as independent constituent quantities. Microscopic couplings between phonons and electrons are described as inhibitory sources in the dual-phase lag (DPL) version [17,18], which results in a delayed reaction at the macroscopic scale. If someone would like to look at how the microstructure affects the macroscopic heat transfer pattern, the DPL thermoelastic mode would be an appropriate model. Empirical results confirm the material implications and integrity of the DPL model [19].

Many research works have been conducted to examine the benefits of Moore–Gibson–Thompson (MGT) equation and its interpretations in recent years. The third-order differential equations, which are ubiquitous in fluid dynamics, form the theoretical basis [20]. Recently, Quintanilla [21,22] developed a new thermoelastic framework for MGT heat transport. By incorporating the relaxation parameters into the GN-III framework, Abouelregal et al. [23–26] created a modified heat transfer equation utilizing the energy equation. In the ideal situations, the thermal shock issue is deterministic, while in the real cases, some noises are present in the context of photo-excitation processes. Lotfy [27] investigated a theoretical method to study the distortion exposed by skewed loads. Sharma and Kumar [28] constructed a dynamic mathematical model for a semiconductor medium. By employing the potential functions, the system of equations for the photo-thermoelastic with dual-phase delay concept was rewritten for two-dimensional cases. Photo-thermoelastic interactions were studied by Kaur et al. [29] in a revolving, infinite, semiconducting solid cylinder subjected to a strong magnetic field operating along its axis. The surface at its border was exposed to a laser pulse with an exponentially varying heat flow. A new generalized theory of Moore–Gibson–Thompson photothermal (MGTPT) model for a semiconductor material was used to express the governing equations. On the other hand, the investigation of photo-thermoelastic interaction in an unbounded semiconductor medium with a spherical cavity was demonstrated by Alzahrani and Abbas [30]. The recently developed hyperbolic two-temperature model addresses this issue well. Using both classical (CT) theory and dual-phase-lag (DPL) model, Gafel [31] calculated how much the starting stress, magnetic field, and fractional parameters, impact the reflection wave within a semiconductor photothermal diffusion medium. In order to characterize the issue at hand, one has to first look at the fundamental sciences, including plasma, thermoelastic waves and the thermomechanical reaction of reflecting photothermal diffusion in the semiconductor components. Within the context of generalized thermodynamics, Ahmed et al. [32] introduced and evaluated a two-dimensional first-order linear system of differential equations for planar strain thermoelasticity. The system comprises the Cattaneo evolution equation for heat transfer and the traditional thermoelastic equations, which uses speeds instead of deformations.

Recently, several studies have been established to deal with the thermoelastic behavior of materials and structures using the modified theories and models by considering different environmental circumstances [33–40]. The contribution of this study is to present a new system of thermo-optical equations that characterize the propagation behavior of photo- and thermal carriers in semiconductors under the intense femtosecond laser pulse excitation. The proposed formulation (4MGT-PTE) is a modified model of Green and Naghdi theory of the third type [14–16] which includes the fourth-order Moore–Gibson–Thompson (MGT) concept. This model allows for limited velocity of wave propagation due to the presence of thermal relaxation. This paper provides some key ideas for extending the thermoelastic theory of homogeneous and isotropic materials. Despite the theoretical nature of the conclusions given in this study, their physical and technical applicability cannot be denied. The fourth-order of 4MGT-PTE model has not been used before to examine the transmission mechanism of thermo-optical waves in semiconductor materials. Moreover, a pulsed laser current would be sent through

the medium results in generating heat and raising the surface temperature. Such models that incorporate the pulsed lasers have superior advantages in various scientific and industrial applications, including the excitation and processing of materials, laser burning, laser cutting, laser engraving, spectroscopy of optical materials as well as dynamic combustion processes.

2 Theoretical model and governing equations

The governing equations of plasma transport coupling under the assumption that the material is homogenous, isotropic, thermoelastic, and photothermal semiconductor can be expressed as [41,42]:

$$(\lambda + \mu)\,\nabla\,(\nabla \cdot \vec{u}) + \mu\nabla^2\vec{u} - \gamma\nabla\theta - d_n\nabla N + \vec{F} = \rho\ddot{\vec{u}} \tag{1}$$

$$D_E\nabla^2 N = \rho\frac{\partial N}{\partial t} + \frac{1}{\tau_B}N + \kappa\theta \tag{2}$$

$$e_{ij} = \frac{1}{2}\left(u_{i,j} + u_{j,i}\right) \tag{3}$$

$$\overline{\overline{\sigma}} = \lambda\,(\nabla \cdot \vec{u})\,\overline{\overline{I}} + \mu\left(\nabla\vec{u} + \nabla\left(\vec{u}^{Tr}\right)\right) - (\gamma\theta + d_n N)\,\overline{\overline{I}} \tag{4}$$

where $\vec{u}$ is displacement vector, N is carrier density, $\theta = T - T_0$ represents the thermodynamical temperature, T_0 is the reference temperature, δ_{ij} stands for the Kronecker's delta, ρ is mass density, $\vec{F}$ denotes the Lorentz force, $\overline{\overline{\sigma}}$ is the stress tensor, $\overline{\overline{I}}$ is the identity tensor, D_E symbolizes the ambipolar diffusion coefficient, E_g is semiconductor gap energy, d_n is the difference in deformation potential of the conduction, κ represents the thermal activation coupling parameter, τ_B shows the bulk free carrier lifetime, $\gamma = (3\lambda + 2\mu)\,\alpha_t$ stands for the volume coefficient of thermal expansion, α_t is the factor of thermal expansion, λ, μ are Lamés constants and e_{ij} is the strain tensor.

According to Fourier's law, the heat flow $\vec{H}$ [W/m^2] at each point within a solid is determined by direction and magnitude of heat gradient. The following equation describes the simplest scenario that can explain the behavior of heat flow:

$$\vec{H}\left(\vec{X}, t\right) = -K\vec{\nabla}\theta\left(\vec{X}, t\right) \tag{5}$$

where K [W/mK] denotes the thermal conductivity coefficient and $\vec{X}$ stands for the position vector.

Here, the following heat-balance equation represents the principle of energy conservation:

$$\rho C_E\frac{\partial\theta}{\partial t} + \gamma T_0\frac{\partial}{\partial t}\,(\nabla \cdot \vec{u}) = -\vec{\nabla} \cdot \vec{H} + Q \tag{6}$$

where C_E [J/kgK] is the specific heat and Q [W/m^3] denotes the heat supply.

The extended Fourier's law can be defined using GN-III concept as follows [15]:

$$\vec{H}\left(\vec{X}, t\right) = -K\vec{\nabla}\theta - K^*\vec{\nabla}\vartheta \tag{7}$$

where the variable ϑ [1/Ks] characterizes the thermal displacement $\left(\dot{\vartheta} = \theta\right)$ and K^* [W/mKs] indicates the rate of thermal conductivity.

We will consider the scenario in which the external light rays excite free electrons in a flexible semiconductor medium, resulting in a carrier-free variation density with energy E_g, which is the gap of the semiconductor. The absorbed optical energy causes a variation in deformation and elastic waves. On the other hand, the thermal-elastic-plasma waves will alter the general form of heat equation. It has been shown that the quantity of light energy absorbed is proportional to the amount of electron-hole recombination occurs. Following is a statement of the modified Fourier's law which is appropriate for semiconductor materials experiencing plasma effects:

$$\vec{H}\left(\vec{X}, t\right) = -K\vec{\nabla}\theta - K^*\vec{\nabla}\vartheta - \int\frac{E_g}{\tau_B}N\mathrm{d}\vec{X} \tag{8}$$

When the energy equation (8) is used in conjunction with the extended Fourier's law of Green and Naghdi framework (GN-III), as described by Eq. (7), it is clear that the hypothesis that considers the heat conduction waves move at a limited speed is implausible. As a consequence, it makes sense to adjust this theory by adding delay or relaxation factors to the traditional equations. When the heat flux's phase lag (relaxation time) is included, the Taylor series approximation may be utilized to derive the approximation of the vector's direction as:

$$\vec{H}\left(\vec{X}, t+\tau_q\right) \approx \left(1+\tau_q \frac{\partial}{\partial t}+\frac{1}{2}\tau_q^2 \frac{\partial^2}{\partial t^2}\right) \vec{H}\left(\vec{X}, t\right) \tag{9}$$

By substituting Eq. (9) into Eq. (8), one obtains the following fourth-order MGT photothermal model:

$$\left(1+\tau_q \frac{\partial}{\partial t}+\frac{1}{2}\tau_q^2 \frac{\partial^2}{\partial t^2}\right) \vec{H} = -K\vec{\nabla}\theta - K^* \vec{\nabla}\vartheta - \int \frac{E_g}{\tau_B} N \mathrm{d}\vec{X} \tag{10}$$

For the rest of this paper, we will assume the following conditions for the constitutive constants:

$$C_E > 0,\ \tau_q > 0,\ K > 0,\ K^* > 0,\ K > \tau_q K^*$$

A positive values of C_E is easy to understand. The stability of solutions for type II/III of Green and Naghdi theories is connected to the assumptions on K and K^*, which are the natural ones. Additionally, it is supposed that τ_q is positive and thought to be small compared to the other constants. The stability of solutions of the MGT problem is often ensured by applying the condition ($K > \tau_q K^*$). The axioms of thermodynamics and the results of experiments are consistent with these hypotheses.

A derivative of the above equation with respect to the coordinate vector $\vec{X}$ and time t yields

$$\left(1+\tau_q \frac{\partial}{\partial t}+\frac{1}{2}\tau_q^2 \frac{\partial^2}{\partial t^2}\right) \frac{\partial}{\partial t}\left(\nabla.\vec{H}\left(\vec{X}, t\right)\right) = -\nabla.\left(K\frac{\partial}{\partial t}\vec{\nabla}\theta\right) - \nabla\left(K^*\vec{\nabla}\theta\right) - \frac{E_g}{\tau_B}\frac{\partial N}{\partial t} \tag{11}$$

By substituting Eq. (11) for the energy conservation equation (6), we obtain the modified fourth-order MGT heat equation that explains the interaction of the thermal-plasma-elastic waves:

$$\begin{aligned}&\left(1+\tau_q \frac{\partial}{\partial t}+\frac{1}{2}\tau_q^2 \frac{\partial^2}{\partial t^2}\right) \frac{\partial}{\partial t}\left[\rho C_E \frac{\partial \theta}{\partial t} + T_0 \frac{\partial}{\partial t}\left(\beta_{ij} e_{ij}\right) - Q\right] \\ &= \nabla.\left(K\nabla\dot{\theta}\right) + \nabla.\left(K^*\nabla\theta\right) + \frac{E_g}{\tau_B}\frac{\partial N}{\partial t}\end{aligned} \tag{12}$$

3 Electromagnetic field equations

Maxwell's Equations are a set of fundamental relationships that regulate the dynamics of electric and magnetic fields and their interactions. The equations characterize the evolution of charge and current, as well as the birth and development of these fields and their interactions with one another. As a result of the presence of primary magnetic field $\vec{H}$, the induced electric field $\vec{E}$ as well as magnetic field $\vec{h}$ will appear in the fundamental equations. The linear simplification of Maxwell's equations that describe the electromagnetic field used in the electrodynamics of an elastic, homogeneously conductive solid, ideally thermally and electrically, is given by the following formulas (ignoring the charge density):

$$\vec{J} = \nabla \times \vec{h} - \varepsilon_0 \frac{\partial \vec{E}}{\partial t}, \quad \nabla \times \vec{E} = -\mu_0 \frac{\partial \vec{h}}{\partial t}, \quad \vec{E} = -\mu_0\left(\frac{\partial \vec{u}}{\partial t} \times \vec{H}\right), \quad \nabla \cdot \vec{h} = 0 \tag{13}$$

where ∇ represents the nabla operator, $\vec{J}$ denotes the current density, μ_0 represents the magnetic permeability, and ε_0 characterizes the electric permeability.

The equation that describes the Maxwell's stress M_{ij} is denoted by:

$$M_{ij} = \mu_0\left[H_i h_j + H_j h_i - H_k h_k \delta_{ij}\right] \tag{14}$$

To calculate the Lorentz force $\vec{F}$ caused by the primary magnetic field $\vec{H}$, one can use the following formula:

$$\vec{F} = \mu_0\left(\nabla \times \vec{H}\right) \tag{15}$$

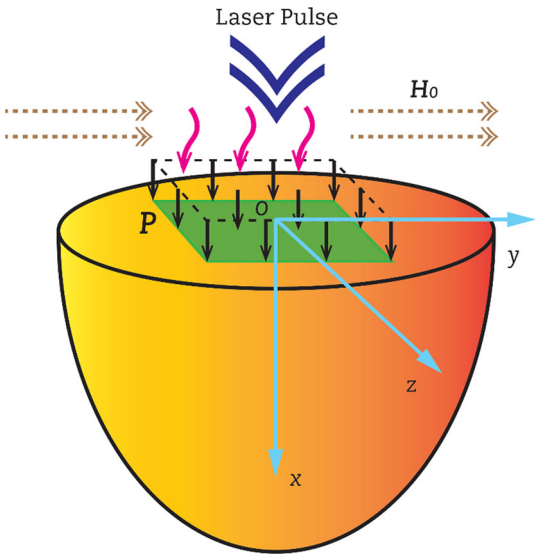

Fig. 1 Schematic representation of a photothermal half-space solid

4 Description of the problem

The problem considered in this work is a two-dimensional thermoelastic solid (half-space) in the region ($x \geq 0$) in which the x-axis is perpendicular to the free surface pointing inside the medium (See Fig. 1). It is assumed that there is a sudden laser pulse that heats the local boundary regions at the free surface $x = 0$ at time $t = 0$. It will also be taken into account that half of the area is affected by a force perpendicular to the boundary surface ($x = 0$) which is variable depending on time and Cartesian coordinates. Since the heating from the laser pulses occurs in a direction perpendicular to the oxz plane, one may treat the proposed problem as a plain strain problem in which all variables depend only on x, z, and t and are independent of y. Finally, the regularity condition are taken into account in the sense that all field variables are constrained away from the surface when x approaches to infinity.

The component of displacement that only affects the x and z directions may be expressed by:

$$\vec{u} \equiv (u(x, z, t), 0, w(x, z, t)) \tag{16}$$

As a result of this equation, one can calculate the dilatation $e = \text{div}\,(\vec{u})$ as:

$$e(xzt) = \frac{\partial u}{\partial x} + \frac{\partial w}{\partial z} \tag{17}$$

The elements of Lorentz force $\vec{F}$ will have the following components when the primary magnetic field $\vec{H}_0 = (0,\ H_0,\ 0)$ is applied:

$$F_x = \mu_0 H_0^2 \left(\frac{\partial e}{\partial x} - \mu_0 \varepsilon_0 \frac{\partial^2 u}{\partial t^2} \right),\ \ F_y = 0,\ \ F_z = \mu_0 H_0^2 \left(\frac{\partial e}{\partial z} - \mu_0 \varepsilon_0 \frac{\partial^2 w}{\partial t^2} \right) \tag{18}$$

When the Lorentz force is considered, the equations of motion (1) in x and z directions have the following formulae, respectively:

$$\left(\lambda + \mu + \mu_0 H_0^2\right) \frac{\partial e}{\partial x} + \mu \nabla^2 u - \gamma \frac{\partial \theta}{\partial x} - d_n \frac{\partial N}{\partial x} = \left(\rho + \varepsilon_0 \mu_0^2 H_0^2\right) \frac{\partial^2 u}{\partial t^2} \tag{19}$$

$$\left(\lambda + \mu + \mu_0 H_0^2\right) \frac{\partial e}{\partial z} + \mu \nabla^2 w - \gamma \frac{\partial \theta}{\partial z} - d_n \frac{\partial N}{\partial z} = \left(\rho + \varepsilon_0 \mu_0^2 H_0^2\right) \frac{\partial^2 w}{\partial t^2} \tag{20}$$

Using Eq. (17) and removing u and w from Eqs. (19) and (20), results in:

$$\left(\lambda + 2\mu + \mu_0 H_0^2\right) \nabla^2 \mathrm{e} - \gamma \nabla^2 \theta - d_n \nabla^2 N = \left(\rho + \varepsilon_0 \mu_0^2 H_0^2\right) \frac{\partial^2 \mathrm{e}}{\partial t^2} \tag{21}$$

In the x–z plane, the coupled plasma wave equation (2) may be expressed as:

$$D_E\left(\frac{\partial^2 N}{\partial x^2}+\frac{\partial^2 N}{\partial z^2}\right)=\rho\frac{\partial N}{\partial t}+\frac{1}{\tau_B}N+\kappa\theta \tag{22}$$

In addition, the heat equation in the modified fourth-order MGT model can be rewritten in the absence of any heat source as

$$\left(1+\tau_q\frac{\partial}{\partial t}+\frac{1}{2}\tau_q^2\frac{\partial^2}{\partial t^2}\right)\left(\rho C_E\frac{\partial^2\theta}{\partial t^2}+\gamma T_0\frac{\partial^2 e}{\partial t^2}\right)=\left(K^*+K\frac{\partial}{\partial t}\right)\left(\frac{\partial^2\theta}{\partial x^2}+\frac{\partial^2\theta}{\partial z^2}\right)+\frac{E_g}{\tau_B}\frac{\partial N}{\partial t} \tag{23}$$

The constitutive equations (4) can be then expressed by:

$$\begin{gathered}\sigma_{xx}=\lambda\frac{\partial w}{\partial z}+(\lambda+2\mu)\frac{\partial u}{\partial x}-(\gamma\theta+d_nN)\\ \sigma_{zz}=\lambda\frac{\partial u}{\partial x}+(\lambda+2\mu)\frac{\partial w}{\partial z}-\gamma\,(\gamma\theta+d_nN)\\ \sigma_{xz}=\mu\frac{\partial u}{\partial z}+\mu\frac{\partial w}{\partial x}\end{gathered} \tag{24}$$

To generalize the numerical simulations, it is useful to consider the nondimensional quantities stated as:

$$\begin{gathered}\left\{x',z',u',w'\right\}=\frac{\eta_0}{c_0}\{x,z,u,w\},\quad t'=\eta_0 t,\quad \left\{\theta',N'\right\}=\frac{1}{\rho c_0^2}\{\gamma\theta,d_nN\},\\ \sigma_{ij}'=\frac{\sigma_{ij}}{\gamma T_0},\ \eta_0=\frac{\rho C_E c_0^2}{K},\ c_0^2=c_1^2+a_0^2,\ c_1^2=\frac{\lambda+2\mu}{\rho},\ c_2^2=\frac{\mu}{\rho},\ a_0^2=\mu_0H_0^2\end{gathered} \tag{25}$$

After removing the prime symbols, the dominant equations (21)–(23) take the following form by inserting the above-mentioned dimensionless variables:

$$\nabla^2 e-\nabla^2\theta-\nabla^2 N=\left(1+\varepsilon_0\mu_0a_0^2\right)\frac{\partial^2 e}{\partial t^2} \tag{26}$$

$$\left(\bar{K}^*+\frac{\partial}{\partial t}\right)\left(\frac{\partial^2\theta}{\partial x^2}+\frac{\partial^2\theta}{\partial z^2}\right)=\left(1+\tau_q\frac{\partial}{\partial t}+\frac{1}{2}\tau_q^2\frac{\partial^2}{\partial t^2}\right)\left(\frac{\partial\theta}{\partial t}+\varepsilon_1\frac{\partial e}{\partial t}\right)-\varepsilon_2\frac{\partial N}{\partial t} \tag{27}$$

$$\left(\frac{\partial^2 N}{\partial x^2}+\frac{\partial^2 N}{\partial z^2}\right)=g_1\frac{\partial N}{\partial t}+g_2N+g_3\theta \tag{28}$$

where

$$\begin{gathered}\varepsilon_1=\frac{\gamma^2T_0}{\rho^2c_0^2C_E},\quad \varepsilon_2=\frac{\gamma E_g}{\rho C_E\tau_Bd_n},\ \bar{K}^*=\frac{K^*}{K\rho c_0^2}\\ g_1=\frac{\rho c_0^2}{D_E\eta_0},\quad g_2=\frac{c_0^2}{D_E\tau_B},\quad g_3=\frac{\kappa d_nc_0^2}{D_E\eta_0^2}\end{gathered} \tag{29}$$

And for Eq. (24) one gets:

$$\begin{gathered}\sigma_{xx}=C_{11}\frac{\partial u}{\partial x}+C_{12}\frac{\partial w}{\partial z}-\theta-N\\ \sigma_{zz}=C_{11}\frac{\partial w}{\partial z}+C_{12}\frac{\partial u}{\partial x}-\theta-N\\ \sigma_{xz}=C_{13}\left(\frac{\partial u}{\partial z}+\frac{\partial w}{\partial x}\right)\end{gathered} \tag{30}$$

where

$$C_{11}=\frac{c_1^2}{c_0^2},\quad C_{12}=\frac{c_1^2-2c_2^2}{c_0^2}C_{13}=\frac{c_2^2}{c_0^2} \tag{31}$$

5 Normal mode technique

The physical variables under consideration have solutions that may be expressed in terms of normal modes using the following formula:

$$\left\{u,\, w,\, \theta, e, N, \sigma_{ij}\right\}(x,z,t) = \mathrm{e}^{(\omega t + iaz)} \left\{u^*,\, w^*,\, \theta^*,\, e^*,\, N^*,\, \sigma_{ij}^*\right\}(x) \tag{32}$$

where the variables $u^*(x)$, $w^*(x)$, $\theta^*(x)$, $\mathrm{e}^*(x)$, $N^*(x)$, and $\sigma_{ij}^*(x)$ are the amplitudes of the studied physical fields. Moreover, $i = \sqrt{-1}$, ω symbolizes the frequency, a symbolizes the wave number in z direction. Applying the normal mode technique to Eqs. (26)–(30) yields:

$$\left(D^2 - \zeta_1\right)\mathrm{e}^* = \left(D^2 - a^2\right)\theta^* + \left(D^2 - a^2\right)N^* \tag{33}$$

$$\left(D^2 - \zeta_2\right)\theta^* = \omega q \varepsilon_1 \mathrm{e}^* - \varepsilon_2 \omega N^* \tag{34}$$

$$\left(D^2 - \zeta_3\right)N^* = g_3 \theta^* \tag{35}$$

$$\begin{aligned} \sigma_{xx}^* &= C_{11} D u^* + iaC_{12} w^* - \theta^* - N^* \\ \sigma_{zz}^* &= iaC_{11} w^* + C_{12} D u^* - \theta^* - N^* \\ \sigma_{xz}^* &= C_{13}\left(iau^* + Dw^*\right) \end{aligned} \tag{36}$$

where

$$\begin{gathered} \zeta_1 = a^2 + \omega^2\left(1 + \varepsilon_0 \mu_0 a_0^2\right), \quad q = \frac{\left(1 + \tau_q \omega + \frac{1}{2}\tau_q^2 \omega^2\right)}{\left(\bar{K}^* + \omega\right)}, \; \zeta_2 = a^2 + q\omega, \\ \zeta_3 = a^2 + g_1 \omega + g_2\,, \; D = \frac{du}{dx} \end{gathered} \tag{37}$$

When the functions $\theta^*(x)$ and $N^*(x)$ are removed from Eqs. (33)-(35), the resulting equation is

$$\left(D^6 - AD^4 + BD^2 - C\right)e^* = 0, \tag{38}$$

with

$$\begin{gathered} A = \zeta_1 + g_7 + \frac{g_6}{g_3}, \quad B = \zeta_1 g_7 + g_8 + a^2 + g_5, \quad C = \frac{a^2 g_5 g_6}{g_3}, \\ g_5 = \zeta_1 - g_3, \quad g_6 = \varepsilon_1 \omega^2 g_3, \quad g_7 = \zeta_2 + \zeta_3, \quad g_8 = \zeta_2 \zeta_3 + \varepsilon_2 \omega^2 g_3. \end{gathered} \tag{39}$$

It is convenient to simplify Eq. (38) by

$$\left(D^2 - k_1^2\right)\left(D^2 - k_2^2\right)\left(D^2 - k_3^2\right)e^* = 0, \tag{40}$$

where k_n^2, $n = 1, 2, 3$ are the solutions of the following polynomial equation

$$k^6 - Ak^4 + Bk^2 - C = 0. \tag{41}$$

The condition of regularity will be considered by ignoring the positive exponent in the physical problem so that the solutions are not infinite when the position approach to infinity. The solution of Eq. (40), which has constraint at $x \to \infty$, may be written as

$$e^*(x) = \sum_{n=1}^{3} C_n \mathrm{e}^{-k_n x} \tag{42}$$

In the same way, one can get

$$\left\{N^*, \theta^*\right\}(x) = \sum_{n=1}^{3} \left\{C_n^{'}, C_n^{''}\right\} \mathrm{e}^{-k_n x} \tag{43}$$

where $C_n^{'}$ and $C_n^{''}$ are two distinct parameters. When Eqs. (42) and (43) are substituted into Eqs. (34) and (35), one gets:

$$C_n^{'}(a,\omega) = H_n C_n, \quad C_n^{''}(a,\omega) = L_n C_n(a,\omega) \tag{44}$$

where

$$H_n = \frac{q\varepsilon_1\omega\left(k_n^2-\zeta_3\right)}{\left(k_n^2-\zeta_1\right)\left(k_n^2-\zeta_3\right)+q\varepsilon_2\omega g_3}, \quad L_n = \frac{q\varepsilon_1\omega g_3}{\left(k_n^2-\zeta_1\right)\left(k_n^2-\zeta_3\right)+q\varepsilon_2\omega g_3} \tag{45}$$

Using Eqs. (42) and (43), and incorporating the nondimensional parameters, one obtains:

$$\left(D^2-k_4^2\right)u^* = \sum_{n=1}^{3} M_n C_n \mathrm{e}^{-k_n x} \tag{46}$$

where

$$k_4^2 = a^2+\omega^2\left(1+\varepsilon_0\mu_0 a_0^2\right),\ M_n = k_n\left(1-H_n-L_n\right) \tag{47}$$

Given the regularity criterion, it is concluded that

$$u^*(x) = C_4\mathrm{e}^{-k_4 x} + \sum_{n=1}^{3}\frac{M_n}{k_n^2-k_4^2}C_n\mathrm{e}^{-k_n x} \tag{48}$$

Substituting from (25), (42), and (48) into (17), and after using nondimensional parameters, leads to:

$$w^*(x) = \tfrac{k_4}{ia}C_4\mathrm{e}^{-k_4 x} + \tfrac{1}{ia}\sum_{n=1}^{3}\left(\tfrac{k_n M_n}{k_n^2-k_4^2}+1\right)C_n\mathrm{e}^{-k_n x} \tag{49}$$

By substituting the above solution into Eq. (36), which stands for the functions u^* w^*, N^* and θ^*, one gets the following:

$$\begin{aligned}
\sigma_{xx}^* &= C_4R_4\mathrm{e}^{-k_4 x} + \sum_{n=1}^{3} R_n C_n \mathrm{e}^{-k_n x}\\
\sigma_{zz}^*(x) &= C_4Q_4\mathrm{e}^{-k_4 x} + \sum_{n=1}^{3} Q_n C_n \mathrm{e}^{-k_n x}\\
\sigma_{xz}^*(x) &= \sum_{n=1}^{3} P_n C_n \mathrm{e}^{-k_n x} + P_4C_4\mathrm{e}^{-k_4 x}
\end{aligned} \tag{50}$$

where

$$\begin{aligned}
R_n &= C_{12}\left(\tfrac{k_n M_n}{k_n^2-k_4^2}+1\right) - C_{11}\left(\tfrac{k_n M_n}{k_n^2-k_4^2}\right) - \left(H_n+L_n\right), \quad R_4 = k_4\left(C_{12}-C_{11}\right),\\
Q_n &= C_{11}\left(\tfrac{k_n M_n}{k_n^2-k_4^2}+1\right) - C_{12}\left(\tfrac{k_n M_n}{k_n^2-k_4^2}\right) - \left(H_n+L_n\right), \quad Q_4 = k_4\left(C_{11}-C_{12}\right),\\
P_n &= -\tfrac{C_{13}}{ia}\left(\tfrac{\left(a^2+k_n^2\right)M_n}{k_n^2-k_4^2}-k_n^2\right), \quad P_4 = -\tfrac{C_{13}}{ia}\left(a^2+k_4^2\right)
\end{aligned} \tag{51}$$

6 Applications

In this part of the article, we will set the unknown parameters C_j, where $j = 1, 2, 3, 4$. It will be taken into account that the initial conditions of the proposed problem is when the half-space is initially at rest. It is assumed that the half-space is affected by a force P perpendicular to the surrounding surface ($x = 0$), which depends on time as well as the spatial coordinate z.

Pulsed laser stimulation causes the temperature to increase or decrease very quickly, or at least in a short time, so very little heat escapes into the surrounding area. As a result, absorption measurements can benefit from pulsed laser excitation. It is also known that when a laser beam illuminates a solid surface, a variety of physical processes may occur, some of which depend on energy. When a medium receives laser radiation, part of the energy is converted into heat. This type of heat generation causes heat waves to propagate through the material with distinct effects (e.g., photothermal effects).

It is also taken into account that the surrounding plane ($x = 0$) of the medium is exposed to laser pulses. In this case, the following thermal condition can be considered:

$$\theta\left(0, z, t\right) = F\left(z, t\right) = \hat{E}\,\hat{\gamma}\left(1 - \hat{R}\right) f\left(z\right) g(t), \tag{52}$$

with $f\left(z\right) = \frac{2}{R_G}\frac{1}{\sqrt{2\pi}} e^{-2z^2/R_G}$ and $g\left(t\right) = \frac{8t^3}{v^2} e^{-2t^2/v^2}$.

For laser heating of materials, it is useful to assume a surface source, as shown in Eq. (52), where $\hat{E}$ is the energy of laser pulse per unit length, $\hat{R}$ is the surface reflectivity, R_G is the radius of the Gaussian beam, v is the rise-time of laser pulse and $\hat{\gamma}$ denotes the extinction coefficient. It is worth mentioning that $\hat{E}$ is the highest amount of light energy that can be produced by a laser during one of its pulses.

On the surface $x = 0$, the mechanical boundary conditions are as follows:

$$\sigma_{zz}\left(0, z, t\right) = -P, \quad \sigma_{xz}\left(0, z, t\right) = 0. \tag{53}$$

As the carriers diffuse, they eventually make it to the sample's surface, where they can undergo recombination with a certain probability. Therefore, the carrier density boundary condition may be stated as follows:

$$D_E \left.\frac{\partial N}{\partial x}\right|_{x=0} = s_f N\left(0, z, t\right) \tag{54}$$

where s_f is the recombination speed near to the surface.

The following equations must be satisfied by parameters C_j $(j = 1, 2, 3, 4)$ are easily obtained by substituting the solutions of variables under consideration into the boundary conditions:

$$L_1C_1 + L_2C_2 + L_3C_3 = F\left(z, t\right)\mathrm{e}^{-(\omega t + iaz)} = P_1 \tag{55}$$

$$R_4C_4 + R_1C_1 + R_2C_2 + R_3C_3 = -P\mathrm{e}^{-(\omega t + iaz)} = -P_0 \tag{56}$$

$$P_4C_4 + P_1C_1 + P_2C_2 + P_3C_3 = 0 \tag{57}$$

$$G_1C_1 + G_2C_2 + G_3C_3 = 0 \tag{58}$$

where $G_n = H_n\left(D_E k_n + s_f\right)$

The matrix form presented below can be used to express the previous set of equations:

$$\begin{Bmatrix} C_1 \\ C_2 \\ C_3 \\ C_4 \end{Bmatrix} = \begin{bmatrix} R_1 & R_2 & R_3 & R_4 \\ P_1 & P_2 & P_3 & P_4 \\ G_1 & G_2 & G_3 & 0 \\ L_1 & L_2 & L_3 & 0 \end{bmatrix}^{-1} \begin{Bmatrix} -P_0 \\ 0 \\ 0 \\ P_1 \end{Bmatrix} \tag{59}$$

After implementing the matrix inverse procedure, the values of four unknown constants C_j, $j = 1, 2, 3, 4\mathrm{j}$ can be obtained. As a result, the solutions are available for deformations, temperature field and any other physical variables of the medium.

7 Discussions on the numerical results

By obtaining the mathematical solutions of different physical quantities, their responses will be determined based on the considered assumptions. The properties of Silicon (Si) material are utilized to illustrate a polymeric semiconductor element for numerical computations. The following value at $T_0 = 298\,\mathrm{K}$ is provided by [43]:

$$\lambda = 2.696 \times 10^{10}\,\mathrm{kg\,m^{-1}s^{-2}}, \quad \mu = 1.639 \times 10^{10}\,\mathrm{kg\,m^{-1}s^{-2}}, \quad \rho = 1740\,\mathrm{kg\,m^{-3}},$$
$$K = 2.510\,\mathrm{W\,m^{-1}\,K^{-1}}, \; C_E = 1.04 \times 10^3\,\mathrm{J\,kg\,K^{-1}}, \; d_n = -9 \times 10^{-31}\,\mathrm{m^3}, \; \omega = 2\,\mathrm{rad\,s^{-1}}$$
$$E_g = 1.5077\,\mathrm{eV}, \quad D_E = 2.5 \times 10^{-3}\,\mathrm{m^2\,s^{-1}}, \quad s_f = 2\,\mathrm{m\,s^{-1}}, \quad \tau = 5 \times 10^{-5}\,\mathrm{s}.$$

The values of the remaining magnetic parameters are assumed to be:

$$\varepsilon_0 = \frac{10^{-9}}{36\pi}\,\mathrm{Fm^{-1}}, \quad \mu_0 = \frac{4\pi}{10^7}\,\mathrm{Hm^{-1}}, \quad H_0 = \frac{10^7}{4\pi}\,\mathrm{Am^{-1}}$$

and it is also supposed that:

$$R_G = 0.45\,\text{mm},\quad v = 10\,\text{ns},\ \hat{R} = 91\%,\ \hat{\gamma} = 0.001\,\text{m}^{-1},\ \hat{E} = 10\,\text{J}$$

Numerical calculations will be done within a very short time, $t = 0.2\,\text{s}$. The above physical constants can be used to describe the distribution of all thermo-optical domains within the semiconducting materials. Furthermore, at plane $z = 0.2$, the profiles of the real part of temperature change $\Re(\theta) = \hat{\theta}$, carrier density $\Re(N) = \hat{N}$, longitudinal displacement $\Re(u) = \hat{u}$ and transverse (tangential) displacement $\Re(w) = \hat{w}$, thermal stress ($\Re(\sigma_{zz}) = \hat{\sigma}_{zz}$ and $\Re(\sigma_{xz}) = \hat{\sigma}_{xz}$) are measured as a function of distance x toward the medium's depth.

7.1 Influence of the laser pulse rise-time parameter

It is known that the rise-time of the picosecond laser pulses is related to both the pulse energy and the spot size, but it is also related to the maximum laser energy density at the silicon surface. The first set of graphs (1-6) shows the effect of the laser pulse rise-time parameter v on the studied system variables versus location x for three different values of v equal to 0.1, 0.2, and 0.3. Boundary requirements are met for all physical quantities, and all curves coincide as x approaches infinity, as seen in the figures. For the range of distances x between 0 and 10, we find that the rise-time parameter v of the laser pulse has a considerable impact (photothermal influence).

The numerical results show that the maximum temperature of the structure is constantly located near the front of the heat wave and gradually declines with rising depth within the medium. The femtosecond laser creates a strange kind of mechanical force. In contrast to continuous or long-pulse laser heat generation, where most of the damage comes from the heat treatment process, femtosecond lasers can make high-quality surfaces with very little damage to other parts. This is because of how mechanical forces are generated and how ultrafast deformation of lattices works. It is clear from this that the photothermal mechanical model, which takes into account all these effects, can explain the ultrafast photothermal response over a range of about three orders of size, from tens of femtoseconds, where electron-to-phonon interactions predominate. Not only that, but it can also explain such behavior down to tens of picoseconds, where phonon-to-phonon interactions predominate.

Figure 2 displays the fluctuation of the temperature change field $\hat{\theta}$ with distance x for the three examples of the rise-time of the laser pulse v. This figure exhibits that the change in temperature $\hat{\theta}$ begins with a maximum positive value at the free surface where the laser pulse is applied and then decreases monotonously, reaching its minimum value at $x = 7$, before gradually decreasing to zero. Regarding the effect of the laser pulse time v on the temperature variation $\hat{\theta}$, it is noted that the laser pulse rises time factor has a very strong influence on the temperature behavior. It is obvious from the Figure that by increasing the parameter v, the size of the temperature field $\hat{\theta}$ becomes larger.

Figure 3 displays the carrier density variation $\hat{N}$ as a function of space x and the pulse rise-time factor v. In each scenario, the carrier density $\hat{N}$ begins with positive values and rises steadily until it reaches its maximum value. The value then declines until it hits zero. The plasma wave propagation, as calculated by the recombination processes, is found to begin with positive values for all three situations of v, as assumed at the surface. Because of this, photo-excitation transport mechanisms make the plasma waves stronger, reaching their peak close to the surface. As you can see in Fig. 2, the laser pulse rise-time parameter v has a big influence on the patterns of carrier density $\hat{N}$. It is detected that the distribution of carrier density $\hat{N}$ declines with the rise of pulse rise-time factor v in the case of the modified 4MGT-PTE photo-thermoelastic theory.

In Fig. 4, we see that the horizontal displacement $\hat{u}$ starts at a maximum and diminishes with increasing distance x and time t. As seen in the figure, the rising time of the laser pulse v has an effect on the amplitude of the component of the displacement $\hat{u}$. Several examples of how the tangential component of displacement $\hat{w}$ varies with the vertical distance x are shown in Fig. 5. For the values $v = 0.101$ and $v = 0.102$, the displacement $\hat{w}$ is noticeably larger than it was for $v = 0.1$, and this is attributed to the existence of the laser pulse rise-time factor v.

The thermal stress aspects $\hat{\sigma}_{zz}$ and $\hat{\sigma}_{xz}$, and their changes as a function of x, are shown in Figs. 6 and 7, respectively. For all three values of the pulse rise-time factor v, the response is qualitatively nearly identical. As the rise-time v of the laser pulse increases, the thermal stress $\hat{\sigma}_{zz}$ and $\hat{\sigma}_{xz}$ components grow in absolute value. In accordance with the boundary criteria, the thermal stress $\hat{\sigma}_{xz}$ component variation always starts with zero. In all three scenarios, the stress $\hat{\sigma}_{zz}$ field first climbs substantially in the early range before gradually decreasing to zero over time. Also, the initial value of stress $\hat{\sigma}_{xz}$ is negative and subsequently declines to the

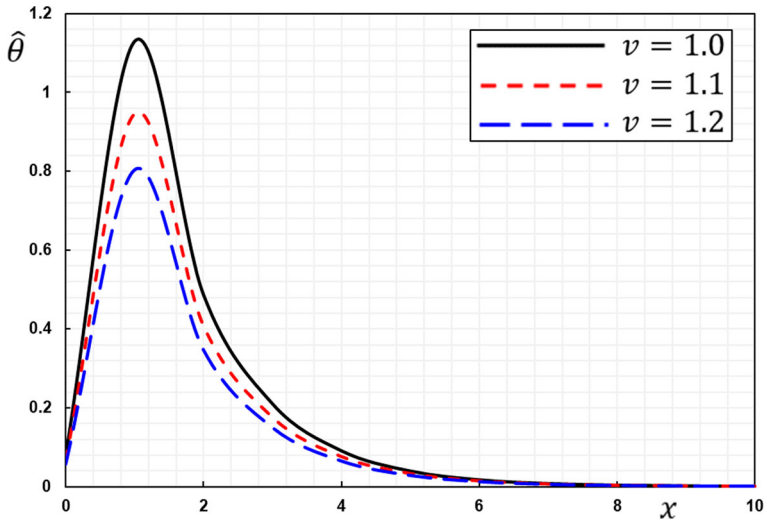

Fig. 2 Variation of temperature $\hat{\theta}$ versus distance x and the laser pulse rise-time v

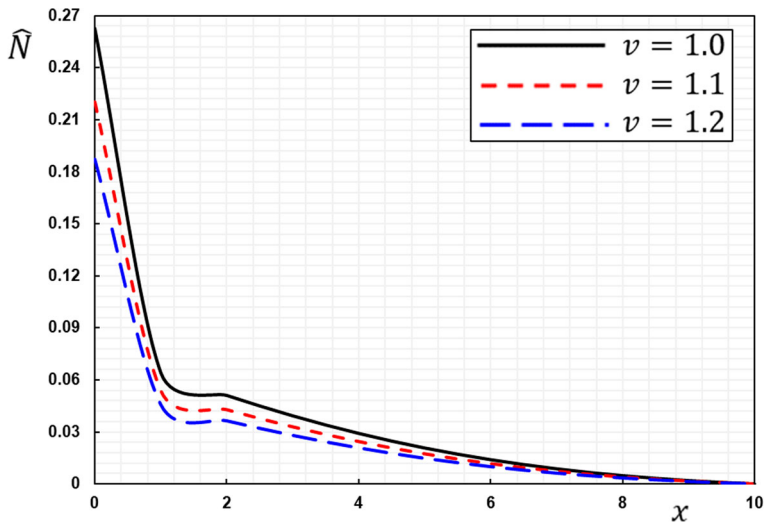

Fig. 3 Carrier charge density $\hat{N}$ versus distance x and the laser pulse rise-time v

minimum value. As can be seen in the graph, the rise-time parameter v of the laser pulse has also resulted in a notable variation in thermal stresses.

It has been shown that valence band electrons in silicon may absorb photon energy and quickly respond to the transition to the conduction band, resulting in the generation of free electrons [44]. This is achieved by using a nanosecond laser with an extremely high-power density. We increased the maximum number of free electrons by using a stronger laser peak power density and shortening the pulse length [45,46]. Silicon absorbs a lot of laser energy, so its intensity gradually decreases as it goes deeper. The narrower pulse width is preferred for more effective silicone treatment with a nanosecond laser. This is because a narrower pulse width results in a larger surface lattice temperature. This numerical analysis can extract important theoretical considerations for selecting a nanosecond laser.

7.2 Analysis of different models of photothermal

A comparative analysis of the various photo-thermoelastic flexible models will be done in this section. The second section developed a new framework based on the fourth-order Moore–Gibson–Thomson (MGT) equa-

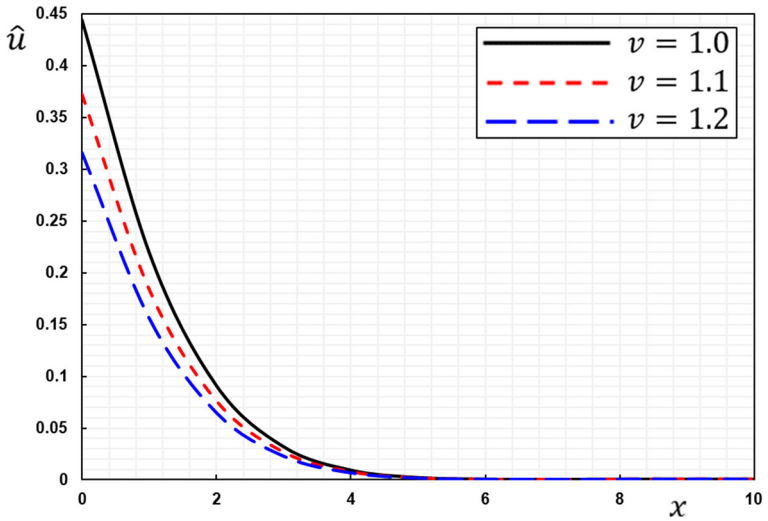

Fig. 4 Variation of displacement $\hat{u}$ versus distance x and the laser pulse rise-time v

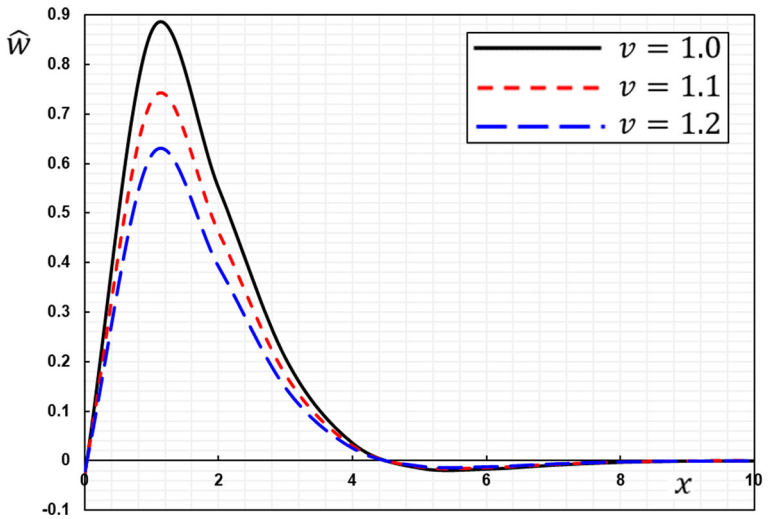

Fig. 5 The tangential displacement $\hat{w}$ versus distance x and the laser pulse rise-time v

tion. The following photothermal frameworks can be derived as special cases from the current developed framework:

- when $\tau_q = 0$ and $K^* = 0$, the usual photo-thermoelasticity model (CTE-PTE) can be obtained.
- Generalized Lord and Shulman photo-thermoelasticity model (LS-PTE).
- When the part incorporating K in the heat equation (12) is omitted, the photothermal model using the Green and Naghdi type II (GNII-PTE) can be derived.
- By setting $\tau_q = 0$ in the heat equation (12), we have the photo-thermoelasticity model using Green and Naghdi's theory of type III (GNIII-PTE).
- In the heat equation (12), when $\tau_q, K^* > 0$ and the second degree of the coefficient τ_q is neglected, the third-order MGT photo-thermoelastic model (3MGT-PTE) can be derived.
- When $\tau_q, K^* > 0$, one has achieved the generalized fourth-order MGT photo-thermoelasticity model (4MGT-PTE).

This subsection presents a list of numerical results in tables to simplify comparisons between different thermoelastic models. The tables could be useful in the future for comparisons in subsequent studies. The results of the differences in the physical photothermal fields will be presented in Tables 1, 2, 3, 4, 5 and 6 and

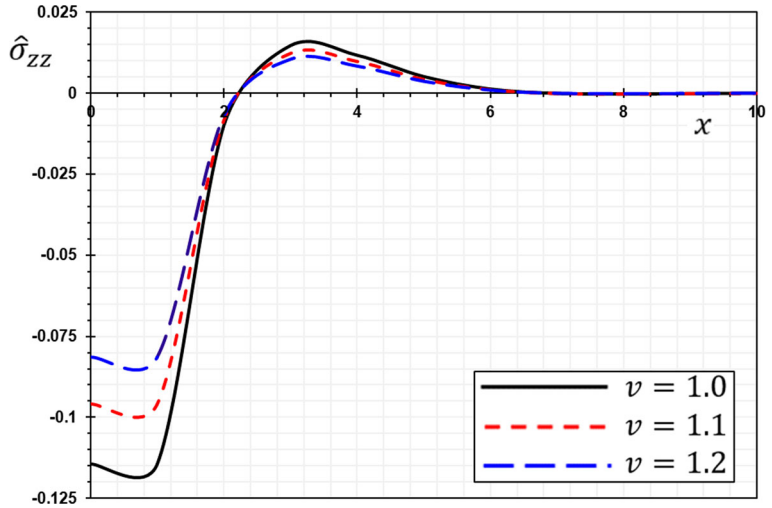

Fig. 6 The normal stress variation $\hat{\sigma}_{zz}$ versus distance x and the laser pulse rise-time v

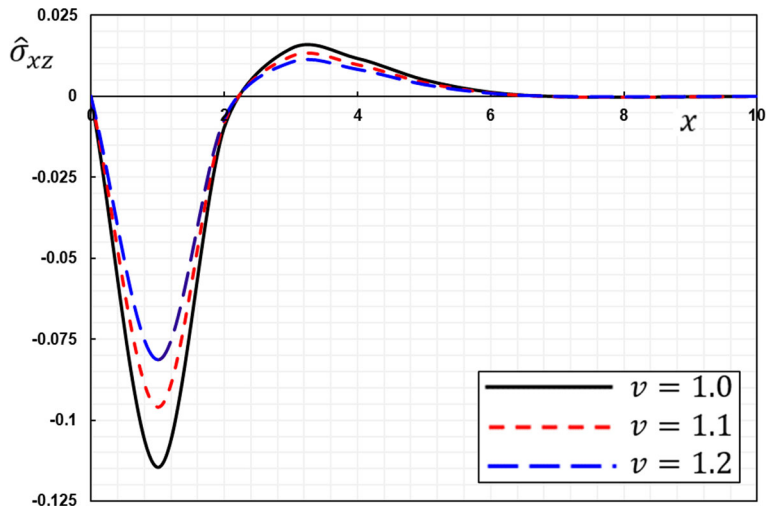

Fig. 7 Variation of tangential stress $\hat{\sigma}_{xz}$ versus distance x and the laser pulse rise-time v

Table 1 The change in temperature $\hat{\theta}$ versus various photothermal models

x	CTE-PTE	LS-PTE	GNII-PTE	GNIII-PTE	3MGT-PTE	4MGT-PTE
0	0.0789221	0.0710299	0.0789221	0.0947065	0.0631377	0.0591916
1	1.31519	0.967239	1.08592	1.42889	0.859764	0.806029
2	0.603624	0.405843	0.458429	0.632967	0.360748	0.338201
3	0.277041	0.170287	0.193528	0.28039	0.151366	0.141905
4	0.127151	0.0714505	0.0816992	0.124206	0.0635114	0.0595419
5	0.0583577	0.0299799	0.0344898	0.0550204	0.0266487	0.0249831
6	0.026784	0.0125792	0.0145601	0.0243728	0.0111815	0.0104827
7	0.0122929	0.0052781	0.0061466	0.0107966	0.0046916	0.00439841
8	0.00564196	0.0022146	0.0025948	0.00478263	0.0019686	0.00184552
9	0.00258945	0.0009292	0.0010954	0.00211859	0.000826	0.00077436
10	0.00118846	0.0003899	0.0004624	0.00093849	0.0003466	0.00032491

Table 2 The variation of displacement $\hat{u}$ versus various photothermal models

x	CTE-PTE	LS-PTE	GNII-PTE	GNIII-PTE	3MGT-PTE	4MGT-PTE
0	0.308286	0.264245	0.286265	0.330306	0.220204	0.198184
1	0.152182	0.130441	0.141312	0.163052	0.108701	0.0978311
2	0.0629635	0.0539687	0.0584661	0.0674609	0.0449739	0.0404765
3	0.0220361	0.0188881	0.0204621	0.0236101	0.01574	0.014166
4	0.00634394	0.0054377	0.0058908	0.00679707	0.0045314	0.00407824
5	0.00141562	0.0012134	0.0013145	0.00151674	0.0010112	0.00091004
6	0.00027984	0.0002399	0.0002599	0.00029983	0.0001999	0.0001799
7	0.00018435	0.000158	0.0001712	0.00019752	0.0001317	0.00011851
8	0.00025531	0.0002188	0.0002371	0.00027355	0.0001824	0.00016413
9	0.00029863	0.000256	0.0002773	0.00031996	0.0002133	0.00019198
10	0.00030777	0.0002638	0.0002858	0.00032975	0.0002198	0.00019785

Table 3 The variation of displacement $\hat{w}$ versus various photothermal models

x	CTE-PTE	LS-PTE	GNII-PTE	GNIII-PTE	3MGT-PTE	4MGT-PTE
0	− 0.02243	− 0.0199373	− 0.0211834	− 0.0249216	− 0.0174451	− 0.0161991
1	0.766372	0.6812190	0.7237960	0.8515240	0.59606700	0.55349100
2	0.489953	0.4355140	0.4627340	0.5443930	0.38107500	0.35385500
3	0.185277	0.1646900	0.1749830	0.2058630	0.14410400	0.13381100
4	0.032793	0.0291493	0.0309711	0.0364366	0.02550560	0.02368380
5	− 0.01255	− 0.011154	− 0.0118511	− 0.0139425	− 0.00975974	− 0.00906261
6	− 0.01451	− 0.0128945	− 0.0137005	− 0.0161182	− 0.01128270	− 0.01047680
7	− 0.00737	− 0.00655484	− 0.00696451	− 0.0081935	− 0.00573548	− 0.00532580
8	− 0.00224	− 0.00198682	− 0.00211100	− 0.0024835	− 0.00173847	− 0.00161429
9	− 0.00012	− 0.00010943	− 0.000116273	− 0.0001368	− 9.57539E−05	− 8.89144E−05
10	0.000334	0.000296709	0.0003152540	0.00037090	0.000259621	0.000241076

Table 4 The values of thermal stress $\hat{\sigma}_{zz}$ versus different photothermal frameworks

x	CTE-PTE	LS-PTE	GNII-PTE	GNIII-PTE	3MGT-PTE	4MGT-PTE
0	− 0.1197519	− 0.0897303	− 0.109142528	− 0.1352601	− 0.08296117	− 0.0762132
1	− 0.102853	− 0.0857108	− 0.0914248	− 0.114281	− 0.0799967	− 0.0742827
2	− 0.0093782	− 0.00781514	− 0.00833615	− 0.0104202	− 0.00729413	− 0.00677312
3	0.0128743	0.0107286	0.0114439	0.0143048	0.0100134	0.00929814
4	0.0103646	0.00863717	0.00921298	0.0115162	0.00806136	0.00748555
5	0.0045409	0.00378409	0.00403636	0.00504545	0.00353181	0.00327954
6	0.00110976	0.000924801	0.000986454	0.00123307	0.000863147	0.00080149
7	− 0.0001027	− 8.55582E−05	− 9.12621E−05	− 0.000114078	− 7.98544E−05	− 7.4151E−05
8	− 0.0002754	− 0.000229481	− 0.00024478	− 0.000305975	− 0.000214182	− 0.00019888
9	− 0.0001652	− 0.000137687	− 0.000146866	− 0.000183582	− 0.000128508	− 0.00011933
10	− 5.933E−05	− 0.000049438	− 5.27338E−05	− 6.59173E−05	− 4.61421E−05	− 4.2846E−05

Table 5 The values of thermal stress $\hat{\sigma}_{xz}$ versus different photothermal frameworks

x	CTE-PTE	LS-PTE	GNII-PTE	GNIII-PTE	3MGT-PTE	4MGT-PTE
0	0	0	0	0	0	0
1	− 0.0370219	− 0.0308516	− 0.0329083	− 0.0411354	− 0.0287948	− 0.026738
2	− 0.226204	− 0.188503	− 0.20107	− 0.251337	− 0.175936	− 0.163369
3	− 0.14453	− 0.120442	− 0.128472	− 0.160589	− 0.112413	− 0.104383
4	− 0.0546297	− 0.0455247	− 0.0485597	− 0.0606996	− 0.0424897	− 0.0394548
5	− 0.00965697	− 0.00804748	− 0.00858397	− 0.01073	− 0.00751098	− 0.00697448
6	0.00370806	0.00309005	0.00329605	0.00412007	0.00288405	0.00267804
7	0.00428046	0.00356705	0.00380485	0.00475607	0.00332925	0.00309144
8	0.00217493	0.00181244	0.00193327	0.00241659	0.00169161	0.00157078
9	0.00065887	0.000549058	0.000585662	0.000732078	0.000512454	0.00047585
10	3.60641E−05	3.00535E−05	0.000032057	4.00713E−05	2.80499E−05	2.60463E−05

Table 6 Carrier charge density $\hat{N}$ versus various photothermal frameworks

x	CTE-PTE	LS-PTE	GNII-PTE	GNIII-PTE	3MGT-PTE	4MGT-PTE
0	0.249642	0.185501	0.2117	0.311908	0.159001	0.145751
1	0.071088	0.0435663	0.0500977	0.079569	0.0373425	0.0342306
2	0.05805	0.034469	0.0396769	0.0638185	0.0295448	0.0270828
3	0.046211	0.0263525	0.0303639	0.0495672	0.0225878	0.0207055
4	0.035821	0.0194163	0.0223921	0.0371912	0.0166426	0.0152557
5	0.026968	0.0137043	0.0158163	0.0268151	0.0117465	0.0107677
6	0.019621	0.00915889	0.0105749	0.0183927	0.00785048	0.00719627
7	0.013679	0.00566304	0.00653723	0.0117702	0.00485404	0.00444953
8	0.008994	0.00307023	0.00353767	0.0067337	0.00263163	0.00241233
9	0.005401	0.0012256	0.0014002	0.0030442	0.00105051	0.000962972
10	0.002728	−2.0225E−05	−4.57167E−05	0.0004611	−1.73353E−05	−1.58907E−05

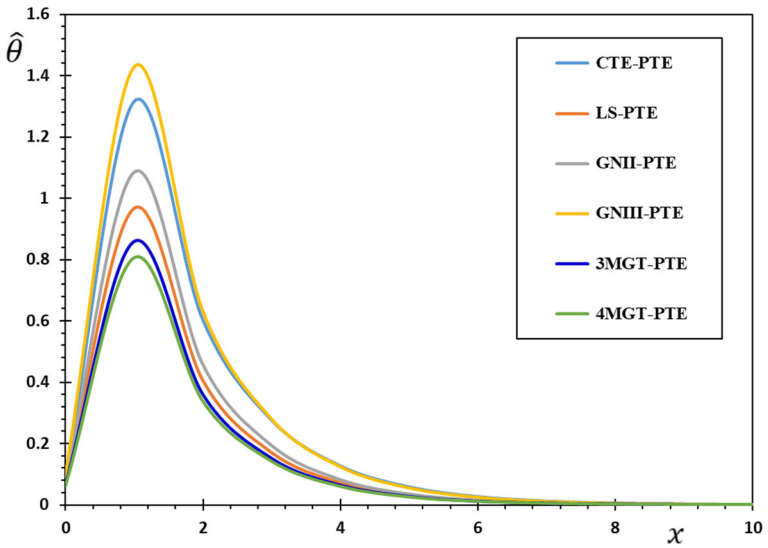

Fig. 8 The variation of temperature $\hat{\theta}$ versus photo-thermoelasticity systems

the curves in Figs. 8, 9, 10, 11, 12 and 13 with the change of vertical distances if the variable z is held at 0.5 and time at $t = 0.12$.

From the tables and figures, the numerical results show that the different field quantity patterns are quite sensitive to the values of the thermal parameters τ_q and K^* as they depend on position and time. Similar behavior curves are obtained around the half-space surface where boundary conditions apply in the case of paired and generalized models and theorems (CTE-PTE, LS-PTE, GNII-PTE, GNIII-PTE, 3MGT-PTE, and 4MGT-PTE). The response changes dramatically when we enter the medium's turbulence region. In contrast to the generalized versions of the propagation of heat waves, these waves move at an infinite speed in the classical photothermal theory (CTE-PTE). This model depicts the interaction of a concentrated laser beam with plasma, heat transfer, and elastic-mechanical waves. Starting with a third-order differential equation and expanding into various concerns relevant to fluid mechanics, the 3MGT-PTE and 4MGT-PTE theories were constructed. When a relaxation factor was taken into account in type III heat transfer, the resulting equation was seen as a thermal conduction equation.

Table 1 and Fig. 8 represent the change in temperature $\hat{\theta}$, we have a prominent contrast between the generalized 3MGT-PTE and 4MGT-PTE theories and GNIII-PTE predictions. The numerical results show that the values for the GNIII-PTE model are greater than for the 3MGT-PTE and 4MGT-PTE photo-thermoelastic models. This proves that the proposed model is correct since it predicts that waves will have limited speeds, while the GNIII-PTE photo-thermoelastic model predicts the opposite. It is also noted that the results of the LS-PTE, 3MGT-PTE, and 4MGT-PTE photothermal models are similar. The reason for this is the introduction of the thermal relaxation time τ_q into the heat conduction equation (12).

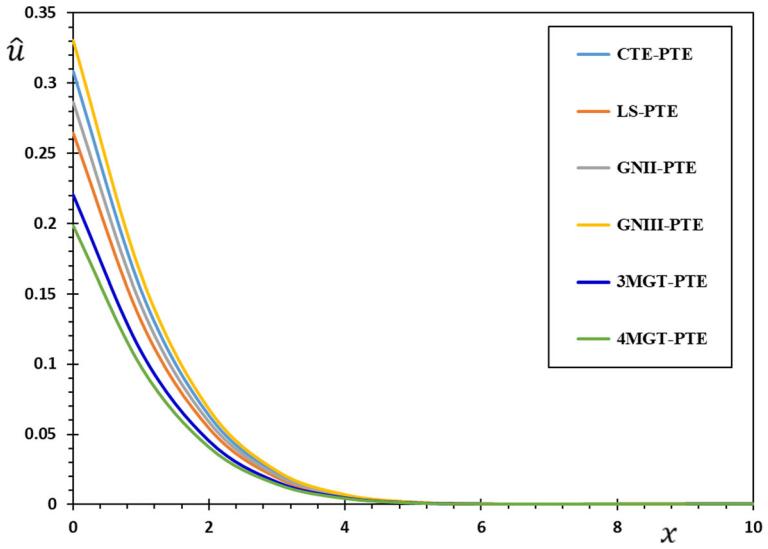

Fig. 9 Change in displacement $\hat{u}$ versus photo-thermoelasticity systems

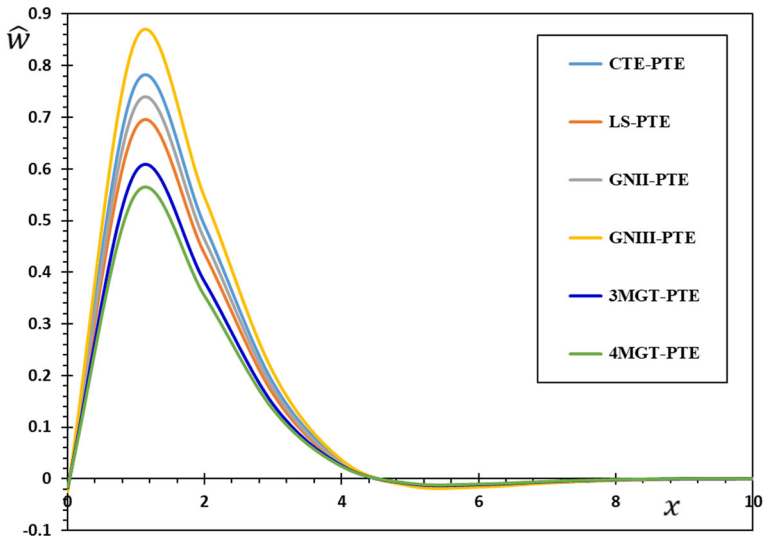

Fig. 10 Change in displacement $\hat{w}$ versus photo-thermoelasticity systems

From the numerical results given in Tables 1, 2, 3, 4, 5, and 6 and also Figs. 8, 9, 10, 11, 12 and 13. The results of the GNIII-PTE generalized photo-thermoelasticity show that they are very different from the ones employed in the GNII-PTE photo-thermoelasticity theory, which relies on a more conservative approach to energy dissipation. Unlike other generalized photo-thermoelastic concepts, the results of the GNIII-PTE model show convergence with the conventional thermoelastic framework CTE-PTE, which does not dissipate heat quickly inside the body, inconsistent with physical phenomena. This is in good agreement with the predictions made by Quintanilla [21,22]. If incorporated into LS-PTE, 3MGT-PTE and 4MGT-PTE photothermal models, the relaxation coefficient might provide more evidence of a temperature reduction. This phenomenon was verified through a series of papers presented by Abouelregal, for example, in [23–26].

It should be noted that the analysis of the third- and fourth-order equations is very different from the analysis of the second-order equation (the traditional photothermal equation ($\tau_q = 0$)), in which the positive thermal relaxation coefficient provides a regulating effect. This is no longer true for quadratic equations of the parabolic type, requiring a different type of analysis than for quadratic equations in thermodynamic equations.

Table 2 and Fig. 9 display the variation in the displacement $\hat{u}$ as a function of distance x. The displacement starts at the lowest, rises to the highest, and finally falls back to zero. When comparing the MGTE conceptual

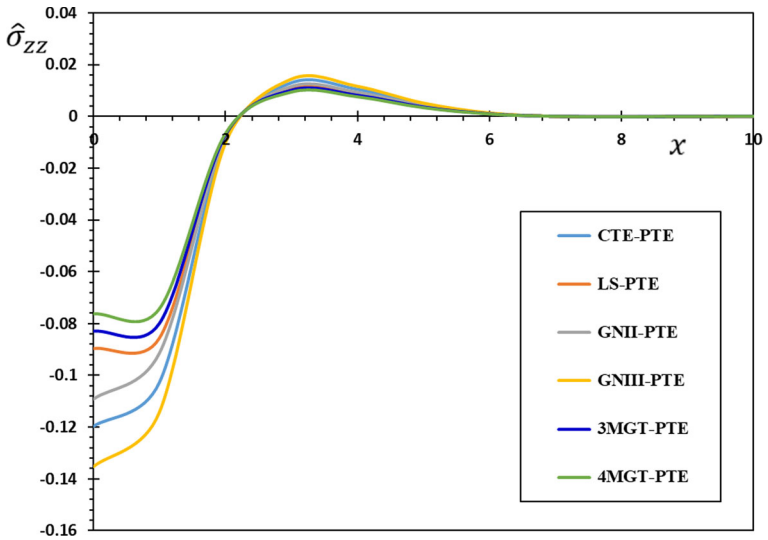

Fig. 11 Change in thermal stress $\hat{\sigma}_{zz}$ versus photo-thermoelasticity systems

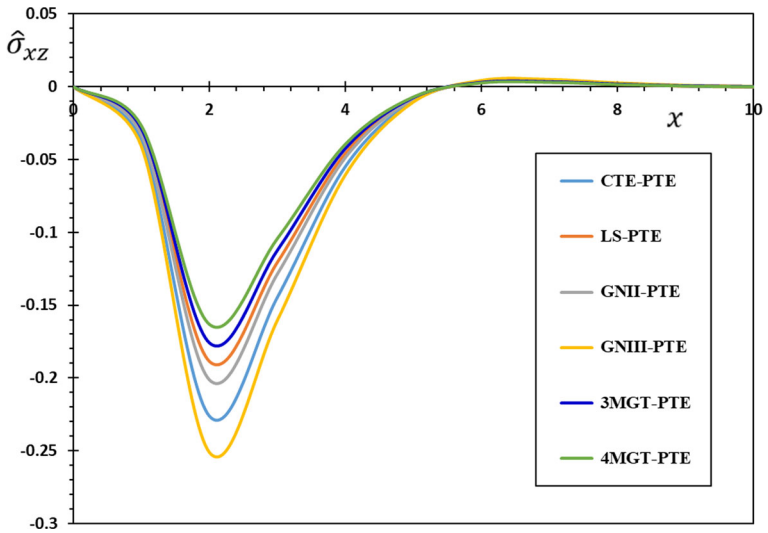

Fig. 12 Change in thermal stress $\hat{\sigma}_{xz}$ versus photo-thermoelasticity systems

framework to the CTE-PTE photo-thermoelastic model, it is shown that the degradation of the displacement occurs more quickly under the 3MGT-PTE and 4MGT-PTE photo-thermoelastic concepts. The GNIII-PTE theory also has a larger displacement than the 3MGT-PTE and 4MGT-PTE frameworks. Also, it was found that the GNIII-PTE, CTE-PTE, 3MGT-PTE, and 4MGT-PTE photo-thermoelastic systems had larger displacement values than the GNII-PTE and LS-PTE systems.

For various photothermal systems, the dispersion behavior of the elastic wave of the displacement $\hat{w}$ pattern versus vertical distance is shown in Table 3 and Fig. 10. In the initial frequency band, the elastic waves are at their highest point and drop dramatically. In contrast, in the second range, the elastic wave first decreases to a minimum value within the photothermal semiconductor half-space before growing again and continuing in this manner until it finds a steady state.

The thermal stress, $\hat{\sigma}_{zz}$, varies as a function of radial distance x as shown in Table 4 and Fig. 11. After increasing it progressively from zero, the maximum negative value is obtained. The reason for this is due to the light energy absorbed in the course of photo-excitation processes. Also, the GNIII-PTE photo-thermoelastic model is demonstrated to have a bigger $\hat{\sigma}_{zz}$ amplitude than any of the alternatives. It is evident from both the table and the Figure that the stress $\hat{\sigma}_{zz}$ profile will decrease when the relaxation constant is present. In the case of the 3MGT-PTE and 4MGT-PTE systems, the generalized thermal elasticity shows that the waves travel

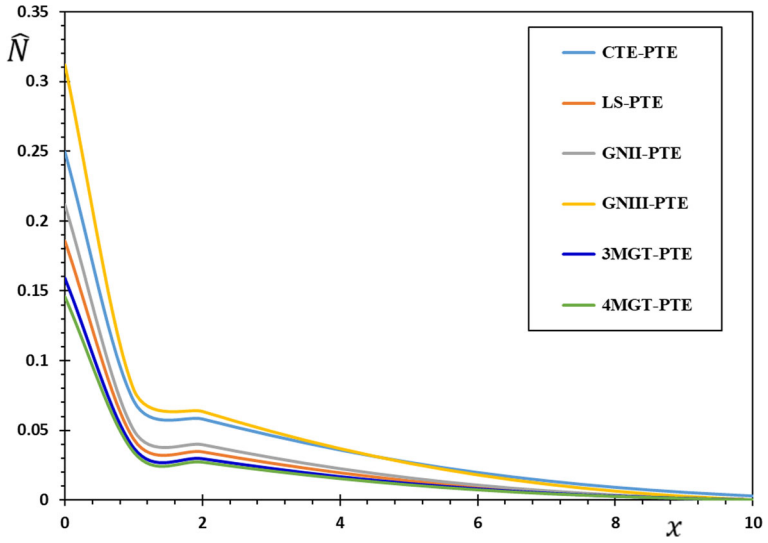

Fig. 13 Change in carrier charge density $\hat{N}$ versus photo-thermoelasticity systems

at finite speeds (Fig. 11 and Table 4). In line with the dynamic stretching phenomenon described above, the tensile stress zone may be observed to grow while the compressed area shrinks.

For an examination of the relationship between the collar stress $\hat{\sigma}_{xz}$ and x for a variety of thermoelastic models, see Table 5 and Fig. 12. From the numerical results, it can be seen that, according to the concept of modified 3MGT-PTE and 4MGT-PTE photo-thermoelastic models, the mechanical waves of the transverse stress $\hat{\sigma}_{xz}$ field travel at finite velocity rates within the half-space in the case of a faster 4MGT-PTE photo-thermoelastic model than in the case of other models. This mechanical wave pattern versus vertical distance for various values of the normal stress distribution $\hat{\sigma}_{xz}$ is depicted in Fig. 12. When applied to a semiconductor surface, the photothermal thermal stress profile is shown to be in accordance with the free mechanical condition. However, in the case of photo-excitation mechanisms, the absorbed optical energy sets the stress distribution to zero. The photothermal stress profile has a minimal value close to the surface and then steadily grows and drops in the second range, eventually reaching a steady state deep into the semiconductor material. It is consistent with physical assumptions that the wave propagations in the various modified photo-thermoelastic models occur at limited speeds.

As shown in Fig. 13 and Table 6, the curves corresponding to different carrier densities $\hat{N}$ show the same behavior with different magnitudes. Based on this graph, the fourth-order Moore–Gibson–Thompson photothermal model (4MGT-PTE) provides the most accurate description of wave propagation in terms of photothermal elastic theory. The carrier density profiles in the 4MGT-PTE photo-thermoelastic theory are much lower in magnitude than those in the CTE-PTE, GNIII-PTE, CTE-PTE, and 3MGT-PTE photo-thermoelastic models. Many contemporary physical issues have solutions that can be found in the MGPT model of the thermoelastic theory of images. On the other hand, the physical field distributions studied in thermo-photovoltaic problems are highly dependent on the 3MGT-PTE and 4MGT-PTE frameworks. All photo-thermoelastic models assume positive values at the surface, as the recombination processes require. Hence, the dispersion of plasma waves is also assumed to be positive, to begin with. Because of this, photo-excitation transport mechanisms make the plasma waves stronger, reaching their peak close to the surface.

It was found that, except for the case of totally degenerate plasma waves at very high temperatures, the relaxation time and the coupling term make the signal weaker and must be considered for accurate measurements of lifetimes and electronic diffusivities. This model has several potential uses in mechanical engineering and alternative energy. Insights gained from this study may help scientists greatly in their quest to improve semiconductor production processes.

8 Concluding remarks

One of the most emerging areas in the field of thermoelasticity is the generalized theory of elasticity with photothermal excitations. Only a few studies corresponding to this hypothesis can be found in the literature.

Since the laser source is limited in width and duration, a thermoelastic model was used to predict these factors. The current study investigated the time-dependent behavior of semiconductor materials with long-range thermoelastic properties and the laser pulse was used to heat the semiconductor material. Since the earlier models somehow fail to predict such materials' behavior appropriately, a new thermoelastic model based on the fourth-order Moore–Gibson–Thompson equation was developed and examined. The proposed thermomechanical model was integrated by combining a hyperbolic partial differential equation for a shift in the displacement field and a similar differential equation for a temperature rise.

The above analysis helped us to conclude that there is a certain region in the semiconductor medium in which all physical variables are non-zero. The numerical values also disappeared uniformly outside this region, indicating no thermal disturbance. The behavior of all physical variables changed due to the presence of a photothermal excitation. According to the temperature profiles, the heat in the medium traveled across it like a wave. It was concluded that the extended thermoelastic theory without energy dissipation is extremely near to the physical properties of elastic materials, confirming that the heat wave front advances at a finite rate in the material as time progresses.

It was established that the rising time of the laser pulse is a crucial element that affects all other fields in a meaningful way. Silicon absorbs a lot of laser energy, so its intensity gradually decreases as it goes deeper. The narrower pulse width is preferred for a more effective silicone treatment with a nanosecond laser. A narrower pulse width results in a larger surface lattice temperature. The reported numerical analysis can extract important theoretical considerations for selecting a nanosecond laser. The distribution of heat stress in the irradiated material is controlled by the amount of heat given in a single laser pulse and how this heat is dispersed in time. Due to the presence of heat stresses, cracking in the material's surface and depth can greatly reduce its ability to tolerate the thermal environment appropriately. For material processing applications where the localized microstructural changes are required at the surface, understanding the effect of heat stress field in a laser irradiated material is crucial (as in laser hardening). Predicting a material's heat stress profile can help fine-tune the other important parameters, such as pulse repetition rate, pulse train duration, peak strength per pulse and depth of focus.

Funding A.E. Abouelregal extends his appreciation to the Deanship of Scientific Research at Jouf University for funding this work through research grant No. (DSR-2021-03-0379). He would also like to thank the College of Science and Arts in Al-Qurayyat for its technical support. H.M. Sedighi is grateful to the Research Council of Shahid Chamran University of Ahvaz for its financial support (Grant No. SCU.EM1401.98).

Declarations

Conflict of interest The authors declared no potential conflicts of interest concerning this article's research, authorship, and publication.

References

1. Sarkisyan, T.V., et al.: Gain and carrier temperature response of semiconductor laser media to short optical pulses. J. Opt. Soc. Am. B **17**, 840–850 (2000)
2. Almoneef, A.A., et al.: Laser short-pulse effect on thermodiffusion waves of fractional heat order for excited nonlocal semiconductor. Adv. Condens. Matter Phys. **2022**, 1523059 (2022)
3. Meyer, J.R., Bartoli, F.J., Kruer, M.R.: Optical heating in semiconductors. Phys. Rev. B **21**, 1559 (1980)
4. Ni, Y., et al.: Research on transient thermal behavior of semiconductor lasers under pulse current excitation by thermoreflection technique. Opt. Commun. **521**, 128540 (2022)
5. Yu, P.Y., Cardona, M.: Fundamentals of Semiconductors: Physics and Materials Properties. Springer, Berlin (2004)
6. Wu, J.: The development and application of semiconductor materials. In: 7th International Forum on Electrical Engineering and Automation (IFEEA), pp. 153–156 (2020)
7. Martynenko, I.V., Litvin, A.P., Purcell-Milton, F., Baranov, A.V., Fedorov, A.V., Gun'ko, Y.K.: Application of semiconductor quantum dots in bioimaging and biosensing. J. Mater. Chem. B **5**(33), 6701–6727 (2017)
8. Huang, X., Liu, C., Zhou, P.: 2D semiconductors for specific electronic applications: from device to system. npj 2D Mater. Appl. **6**, 51 (2022)
9. Sahu, M.K.: Semiconductor nanoparticles theory and applications. Int. J. Appl. Eng. Res. **14**(2), 491–494 (2019)
10. El-Sapa, S., et al.: Moore–Gibson–Thompson theory of a non-local excited semiconductor medium with stability studies. Alex. Eng. J. **61**, 11753–11764 (2022)
11. Biot, M.A.: Thermoelasticity and irreversible thermodynamics. J. Appl. Phys. **27**, 240–253 (1956)
12. Lord, H.W., Shulman, Y.: A generalized dynamical theory of thermoelasticity. J. Mech. Phys. Solids **15**, 299–309 (1967)

13. Green, A.E., Lindsay, K.: Thermoelasticity. J. Elast. **2**, 1–7 (1972)
14. Chirilă, A., Marin, M., Montanaro, A.: Well-posedness for thermo-electro-viscoelasticity of Green–Naghdi type. Contin. Mech. Thermodyn. **34**, 39–60 (2022)
15. Marin, M., Öchsner, A., Craciun, E.M.: A generalization of the Gurtin's variational principle in thermoelasticity without energy dissipation of dipolar bodies. Contin. Mech. Thermodyn. **32**, 1685–1694 (2020)
16. Del Piero, G.: A mechanical model for heat conduction. Contin. Mech. Thermodyn. **32**, 1159–1172 (2020)
17. Abouelregal, A.E., et al.: Computational analysis of an infinite magneto-thermoelastic solid periodically dispersed with varying heat flow based on non-local Moore–Gibson–Thompson approach. Contin. Mech. Thermodyn. **34**, 1067–1085 (2022)
18. Jalaei, M.H., Thai, H.T., Civalek, Ö.: On viscoelastic transient response of magnetically imperfect functionally graded nanobeams. Int. J. Eng. Sci. **172**, 103629 (2022)
19. Tzou, D.Y.: Experimental support for the lagging behavior in heat propagation. J. Thermophys. Heat Transf. **9**, 686–693 (1995)
20. Lasiecka, I., Wang, X.: Moore–Gibson–Thompson equation with memory, part II: general decay of energy. J. Differ. Equ. **259**, 7610–7635 (2015)
21. Quintanilla, R.: Moore–Gibson–Thompson thermoelasticity. Math. Mech. Solids **24**, 4020–4031 (2019)
22. Quintanilla, R.: Moore–Gibson–Thompson thermoelasticity with two temperatures. Appl. Eng. Sci. **1**, 100006 (2020)
23. Abouelregal, A.E., et al.: Thermoelastic processes by a continuous heat source line in an infinite solid via Moore–Gibson–Thompson thermoelasticity. Materials **13**, 4463 (2020)
24. Aboueregal, A.E., Sedighi, H.M.: The effect of variable properties and rotation in a visco-thermoelastic orthotropic annular cylinder under the Moore–Gibson–Thompson heat conduction model. Proc. Inst. Mech. Eng. Part L J. Mater. Des. Appl. **235**, 1004–1020 (2021)
25. Alfadil, H., et al.: Effect of the photothermal Moore–Gibson–Thomson model on a rotating viscoelastic continuum body with a cylindrical hole due to the fractional Kelvin–Voigt model. Ind. J. Phys. (2022). https://doi.org/10.1007/s12648-022-02434-9
26. Abouelregal, A.E., Ersoy, H., Civalek, O.: Solution of Moore–Gibson–Thompson equation of an unbounded medium with a cylindrical hole. Mathematics **9**, 1536 (2021)
27. Lotfy, K., Ahmed, A., El-Bary, A., Tantawi, R.S.: A novel stochastic model of the photo-thermoelasticity theory of the non-local excited semiconductor medium. Silicon (2022). https://doi.org/10.1007/s12633-022-02021-x
28. Sharma, N., Kumar, R.: Photo-thermoelastic investigation of semiconductor material due to distributed loads. J. Solid Mech. **13**, 202–212 (2021)
29. Kaur, I., Singh, K., Craciun, E.-M.: A mathematical study of a semiconducting thermoelastic rotating solid cylinder with modified Moore–Gibson–Thompson heat transfer under the Hall effect. Mathematics **10**(14), 2386 (2022)
30. Alzahrani, F.S., Abbas, I.A.: Photothermal interactions in a semiconducting media with a spherical cavity under hyperbolic two-temperature model. Mathematics **8**(4), 585 (2020)
31. Gafel, H.S.: Fractional order study of the impact of a photo thermal wave on a semiconducting medium under magnetic field and thermoplastic theories. Inf. Sci. Lett. **11**, 629–638 (2022)
32. Ahmed, E.A.A., El-Dhaba, A.R., Abou-Dina, M.S., Ghaleb, A.F.: On a two-dimensional model of generalized thermoelasticity with application. Sci. Rep. **12**, 15562 (2022)
33. Abouelregal, A.E., Mohammad-Sedighi, H., Faghidian, S.A., Shirazi, A.H.: Temperature-dependent physical characteristics of the rotating nonlocal nanobeams subject to a varying heat source and a dynamic load. Facta Univ. Ser. Mech. Eng. **19**(4), 633–56 (2021)
34. Fahmy, M.A.: A novel BEM for modeling and simulation of 3T nonlinear generalized anisotropic micropolar-thermoelasticity theory with memory dependent derivative. Comput. Model. Eng. Sci. **126**(1), 175–99 (2021)
35. He, C.H., Liu, C., He, J.H., Mohammad-Sedighi, H., Shokri, A., Gepreel, K.A.: A fractal model for the internal temperature response of a porous concrete. Appl. Comput. Math. **21**(1), 71–77 (2022)
36. Atta, D.: Thermal diffusion responses in an infinite medium with a spherical cavity using the Atangana-Baleanu fractional operator. J. Appl. Comput. Mech. **8**(4), 1358–1369 (2022)
37. Gu, B., He, T., Ma, Y.: Scale effects on thermoelastic coupling wave propagation of micro-beam resonator using nonlocal stain gradient and generalized thermoelasticity. Int. J. Appl. Mech. **13**(09), 2150103 (2021)
38. Sladek, J., Sladek, V., Repka, M.: The heat conduction in nanosized structures. Phys. Mesomech. **24**, 611–617 (2021)
39. Govindarajan, S.G., Solbrekken, G.L.: Non-dimensional thermoelastic model of a compound annular cylinder in a stress-free state with internal heat generation. Proc. Inst. Mech. Eng. C J. Mech. Eng. Sci. **235**(19), 4314–26 (2021)
40. Awwad, E., Abouelregal, A., Hassan, A.: Thermoelastic memory-dependent responses to an infinite medium with a cylindrical hole and temperature-dependent properties. J. Appl. Comput. Mech. **7**(2), 870–882 (2021)
41. Chen, W., Ikehata, R.: The Cauchy problem for the Moore–Gibson–Thompson equation in the dissipative case. J. Differ. Equ. **292**, 176–219 (2021)
42. Todorović, D.M.: Plasma, thermal, and elastic waves in semiconductors. Rev. Sci. Instrum. **74**, 582–585 (2003)
43. Song, Y.Q., Bai, J.T., Ren, Z.Y.: Study on the reflection of photothermal waves in a semiconducting medium under generalized thermoelastic theory. Acta Mech. **223**, 1545–1557 (2012)
44. Othman, M.I.A., Tantawi, R.S., Eraki, E.E.M.: Effect of rotation on a semiconducting medium with two-temperatures under LS theory. Arch. Thermodyn. **38**, 101–122 (2017)
45. Rämer, A., Osmani, O., Rethfeld, B.: Laser damage in silicon: energy absorption, relaxation, and transport. J. Appl. Phys. **116**, 053508 (2014)
46. Yang, J., et al.: The effect of different pulse widths on lattice temperature variation of silicon under the action of a picosecond laser. Micromachines **13**, 1119 (2022)